J Mater Sci (2009) 44:6078–6089
DOI 10.1007/s10853-009-3839-3

Structure–property interface correlation of fly ash–*isotactic* polypropylene composites

Dilip Chandra Deb Nath · Sri Bandyopadhyay · Aibing Yu · Qinghua Zeng · Tapas Das · Darryl Blackburn · Chris White

Received: 7 July 2009 / Accepted: 21 August 2009 / Published online: 4 September 2009

Abstract Composites of *isotactic* semicrystalline polypropylene (PP) reinforced with fly ash (FA) particles (particle size 5–60 μm) were prepared by injection moulding at 210 °C incorporating 20, 45 and 60% by weight of fly ash. Tensile tests were carried out at 25, 50 and 70 °C. WAXRD, DSC and SEM studies were also undertaken. Modulus of elasticity of all composites at all temperatures was higher than that of the corresponding PP samples—the gain ranged between 10 and 60%. The strength of the composites had a mixed trend. At 25 °C, the composites suffered significant loss in strength, as much as 47%, whereas, at 50 and 70 °C, there was up to 15% gain in strength. Strain to failure of the composite samples ranged from as low as 6% at 25 °C to over 50% at 70 °C, coinciding with increase of Pukanszky parameter from 1.5 to 4.1. WAXRD and DSC tests confirm that FA is nucleator of β-crystalline phase the amount of which increases to a maximum of 11% with increasing FA. SEM studies indicated that the polymer had a distinctly high lamellar ductility and showed interfacial interaction with FA in 20% FA composites at 50 and 70 °C. The –OH group on the surface of FA appears responsible for the formation of interfacial interaction with PP chain. Notched Charpy tests showed a maximum gain of 58% impact energy for the composite with 45% FA, tested at 70 °C over that of pure PP at 25 °C.

D. C. D. Nath · S. Bandyopadhyay (✉) · A. Yu · Q. Zeng
School of Material Science and Engineering, The University of New South Wales, Kensington, NSW 2052, Australia
e-mail: S.Bandyopadhyay@unsw.edu.au

T. Das · D. Blackburn · C. White
Research and Ash Development, Cement Australia, Darra, QLD 4076, Australia

Introduction

There is increasing pressure to reuse industrial by-products that have been discarded in the past. Coal-burning power stations generate amount of fine powder by-product, known as fly ash (FA). The storage and handling of FA are challenging tasks that affect the cost effectiveness of the relevant industry. The landfill method is mainly used to dispose FA in ash dams and lagoons. Research on recycling and reuse of FA has lately become an interesting field of study in the emerging markets for green and eco-friendly manufacturing processes and products [1].

There are several interrelated factors, which influence FA properties, including the nature of the coal, coal preparation before firing, the firing system, the method of collection and any subsequent processing. Knowledge of surface morphology and elemental composition of FA are of importance for incorporating them into metal, ceramic or polymer. Optical microscopy (OM), scanning electron microscopy (SEM), transmission microscopy (TEM), atomic force microscopy (AFM) as well as wide-angle X-ray diffraction (WAXRD) have extensively been utilised to characterize the macro- and micro-structural features of the surface of FA [2–4]. Chemically, FA itself is principally a mixture of alkali and transition metal oxides mainly of silicon, aluminium and iron, and small percentage of oxides of calcium, magnesium, potassium, sodium, titanium depending on the processing and coal composition [5].

Fly ash is currently used in the production of cement, concrete, liquid waste stabilization, hydraulic mine backfill, mining application, road constructions and as fertilizer in paddy field [6, 7]. Recent research has used FA as filler/reinforcing material in metal [8] and polymer matrix such as polyester [9], epoxy [10] and PP [11–14]. Whilst PP is a very attractive thermoplastic with moderately high strength

and elevated temperature capability, however, the tensile strength of PP–FA composite materials decreased with the addition of FA [11]. In contrast, the use of naturally abundant particle type clays as reinforcement in PP has increased its strength because of the smaller size particles of clays causing a much better dispersion [15].

The resulting mechanical properties of composites generally depend on the filler's nature, size and distribution, aspect ratio, volume fraction, and the intrinsic adhesion between the surfaces of filler and polymer [16]. High aspect ratio (fibre type) fillers generally increase the yield strength because the filler is capable of attaining high local stress transferred from the polymer matrix [17], which does not happen with lower aspect ratio fillers such as FA. The reduced tensile strength in particulate fillers such as fly ash may arise from, (a) poor adhesion at the interface of the filler and the polymer, and (b) generation and growth of cracks in the particle and subsequent splitting of the composites [17, 18].

Despite the above-mentioned drawbacks, fly ash-reinforced PP composites can still find numerous engineering applications particularly at elevated temperatures, where the fly ash becomes a source of strength whilst the polymer provides enhanced ductility. One major environmental value of using the already available huge quantities of fly ash is that it can lead to conservation of other regular filler materials routinely used in polymers in significant proportions [19].

The main objectives of the current research topis were to

(a) make PP–FA composites and evaluate mechanical properties as a function of FA content at testing temperatures leading to 70 °C.
(b) undertake a mechanistic study of the mechanical properties in terms of (i) the microstructure and morphology and (ii) calculation of interfacial interaction parameter between surfaces of FA and PP.

Experimental

Materials and sample preparation

(a) Fly ash sample was generated in Gladstone Coal Fire Power Plant and supplied by Cement Australia, Queensland. (The typical physical and chemical characteristics of FA are described in section "Results and discussion").
(b) The white powdery type PP was procured from Martogg Company Ltd. Sydney, Australia. The ASTM D1505-03, 10 min melt flow index (MFI) of the PP is 60, indicating a low viscosity grade resin, which is suitable for injection moulding.
(c) PP–FA tensile samples of ASTM-638 type A designation were fabricated by injection moulding in a Boy 15 S equipment at 210 °C from a 72-h ball mill premixed mixture of PP with FA concentrations of (a) 20, (b) 45 and (c) 60 wt%. Pure PP tensile sample was also prepared injection moulding under similar conditions.
(d) Charpy notched specimens according to ASTM D256 were prepared by injection moulding with dimensions: 128 × 13 × 4 mm^3; notch in the centre on one side with width 11 mm; angle 45° and notch root radius 0.25 mm.

Testing and analytical instruments

(a) Coulter Light Scattering Particle Size Analyser (CLSPSA) was used to determine the particle size and size distribution of FA, using water as a fluid, and the experiment being run for 60 s.
(b) The chemical composition of FA was obtained using the Inductively Coupled Plasma Atomic Emission spectroscopy (ICP-AES) and X-ray Fluorescence Spectroscopy (XRF).
(c) Tensile properties were determined using an Instron 1122 5kN testing machine with crosshead movement 5 mm/min at 25, 50 and 70 °C using temperature-controlled furnace chamber. The specimens were placed inside the furnace and allowed time to stabilize to the desired temperature, and the load–displacement data was collected using a Picolog ADC100 Datalogger attached to instrument. The crosshead displacement time data was converted to strain (%) with crosshead speed and initial length of sample. Because of tensile testing inside the furnace enclosure, optical extensometer could not be used to measure Young's modulus accurately. The modulus of elasticity of the sample was calculated from the slope of the tensile stress versus strain (%) as calculated by the computer.
(d) Thermal analysis, i.e. melting and crystallisation studies were conducted using Perkin Elmer Differential Scanning Calorimetry (DSC) TAC-7/DX under nitrogen atmosphere at 10, 15 and 20 °C heating rate in the range of −30 °C to 200 °C, and hold 2 min at 200 °C to remove all the thermal history properly. About 10–14 mg sample was sealed in a 30 μL aluminium pan, another empty aluminium pan was used as the reference. The second heating peaks were taken to evaluate melting temperatures of PP and PP–FA composites.
(e) Wide angle X-ray diffraction (WAXRD) was carried out to investigate the structure of FA, PP and the composites. This was conducted in a multipurpose

diffraction (MPD-Scherrer) with diffracted beam graphite monochromators using Ni filtered Cu Kα radiation. Diffractometer conditions for data collection were set to 40 kV and 20 mA, 2θ scanning range from 5°–90° with step size 0.02, time per step 0.5 s. Qualitative phase analysis of FA was performed using the search/match X-Pert software program.

(f) X-ray Photoelectron Spectroscopy (XPS) experiment was undertaken for determination of hydroxyl concentration on FA surface in a vacuum generator instrument model Escalb 220-IXL with resolution of 0.8 eV at 240 W (Al Kα, 12 kV).

(g) Finally, Charpy V-notched Impact test was carried out using Toyoseiki, Tokyo Charpy tester—angle in raised position of pendulum was 135° with striking velocity 2.4 m/s. Like the tensile specimens, impact test was also performed at 25, 50 and 70 °C. The samples were heated to desired temperature in a furnace, held for 1 h and then transferred to the impact tester through a temperature-controlled thermal flask to maintain the temperature. The transfer from the thermal flask to the impact tester, and carrying out the impact test did not take any more than 10 s, which is believed to be an acceptable limit. Three specimens were tested for each condition. Average energy of closest two values was evaluated as the impact energy.

Results and discussion

Physical and chemical characterization of FA

The bimodal peak recorded by CLSPSA in Fig. 1 shows a wide ranges 5–70 μm of particle size distribution of FA. The majority of FA particles were in the size around 40 μm. The result of this analysis was supported by SEM micrograph in Fig. 2, which displays the different sizes of spherical particles. Although some small sizes particles were deposited to the surfaces of bigger particles and inter-particles agglomeration were observed, the irregularly shaped amorphous particles were not appeared in this FA. This type of irregularly shaped amorphous particles was generated in rapid cooling and combustion temperature [4]. Table 1 shows chemical composition of fly ash as analysed by ICP-AES and XRF, confirming that the FA is a mixture of alkali, alkaline and transition metal oxides. The ratio of SiO_2, Al_2O_3, Fe_2O_3 and CaO are slightly different in the two methods: 47, 31, 15 and 2 for ICP-AES, whereas it is 47, 29, 12 and 5 by XRF. The percentage of the minor compounds in FA is almost the same using the two methods.

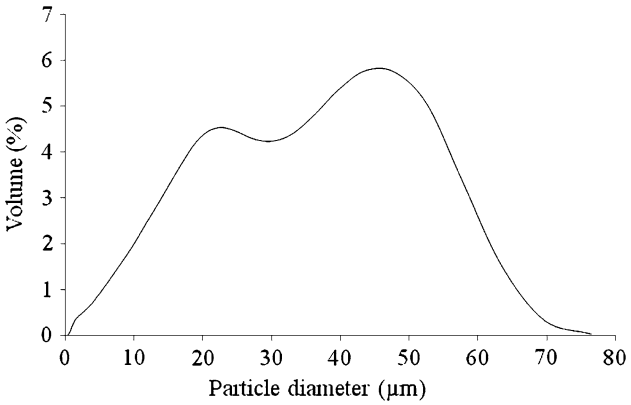

Fig. 1 Particle size distribution pattern of FA, as analysed by CLSPASA technique

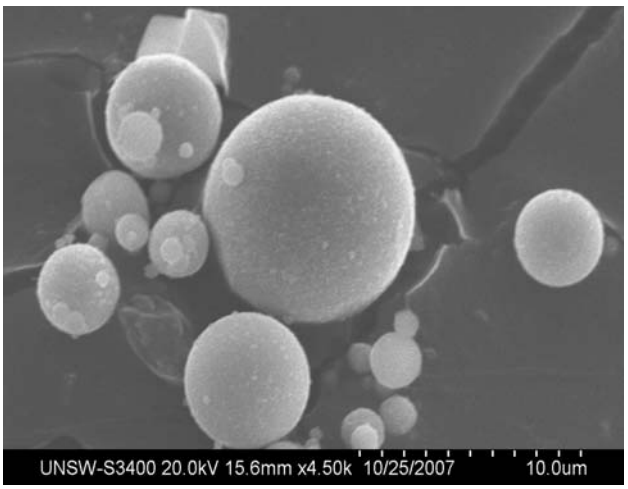

Fig. 2 SEM image of spherical morphology of FA

Table 1 Chemical composition of fly ash analysed by two different methods

Compounds	Analysed by ICP-AES	Analysed by XRF
SiO_2	47.00	47.27
Al_2O_3	31.10	28.96
Fe_2O_3	15.10	11.46
CaO	1.50	5.03
MgO	1.10	1.48
TiO_2	2.20	1.48
BaO	0.02	–
Cr_2O_3	0.05	–
K_2O	0.12	0.80
MnO	0.24	0.17
Na_2O	0.13	0.77
P_2O_5	0.09	1.00
SrO	0.01	–
LOI	0.92	1.65
	100%	100%

Mineralogical characterization of FA

Results of the constituent phases of FA and composites with PP obtained by WAXRD are shown in Fig. 3. Comparison with standard reference by search and match method using X-Pert software indicates the contents of FA to be 68.7% orthorhombic mullite (aluminium silicate, $3Al_2O_3{\cdot}2SiO_2$) (essentially a type of glass), 23.2% hexagonal quartz (silicon oxide, SiO_2), and 8.1% of hematite (Fe_2O_3). The QEMSCAN simulation analysis revealed that FA contains 70% aluminium-silicate mullite and 10% silica phase, with various metal oxides constituting the balance. It may be noted that mullite basically, is not a major ingredient in coal. It forms in the process of thermal decomposition of natural mineral kaolinite present in coal by a series of chemical reactions [13].

Thermal properties of PP–FA composites

The DSC scans of the materials in Fig. 4, show mainly mono-modal peak of monoclinic α-crystalline phase [20] for neat PP. With increasing FA addition, the appearance of pseudo hexagonal β-phase becomes increasingly pronounced. Whilst in these composites FA is seen as a heterogeneous β nucleator, a number of papers have reported similar phenomena but using different fillers, e.g. calcium carbonate, quinacridon dye and wollastonite [16, 21], talc [22], kaolin [23], carbon black [24], calcium carbonate [25], clay [26], ZnO [27], glass fiber [28], silica [29] and carbon nanotube [30].

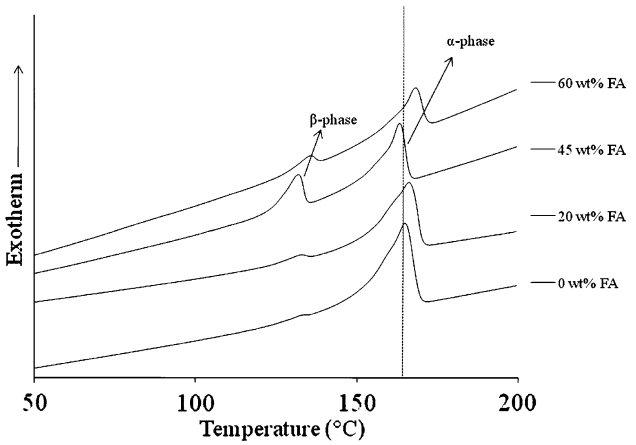

Fig. 4 DSC chart of melting behaviour of PP and composites at heat rate 10 °C/min

For the PP–FA composites of Fig. 4, Table 2 presents the melting point, enthalpy, and calculated percentage crystallinity using Eq. 1.

$$X_{c(\%)} = (\Delta H_m/\Delta H) \times 100 \quad (1)$$

where ΔH_m is the enthalpy of melting of samples and ΔH is the enthalpy of melting of 100% α- or β-crystalline phase taken as 178 J/mg for α, and 168 J/mg for β forms [31].

The following points are worth noting in Table 2:

(a) The maximum level of β form crystallinity has been achieved is 11% by 45% FA addition.
(b) As more and more fly ash is added, the molar fraction of the neat PP goes down, which results in a decrease in melting enthalpy values for the composites.

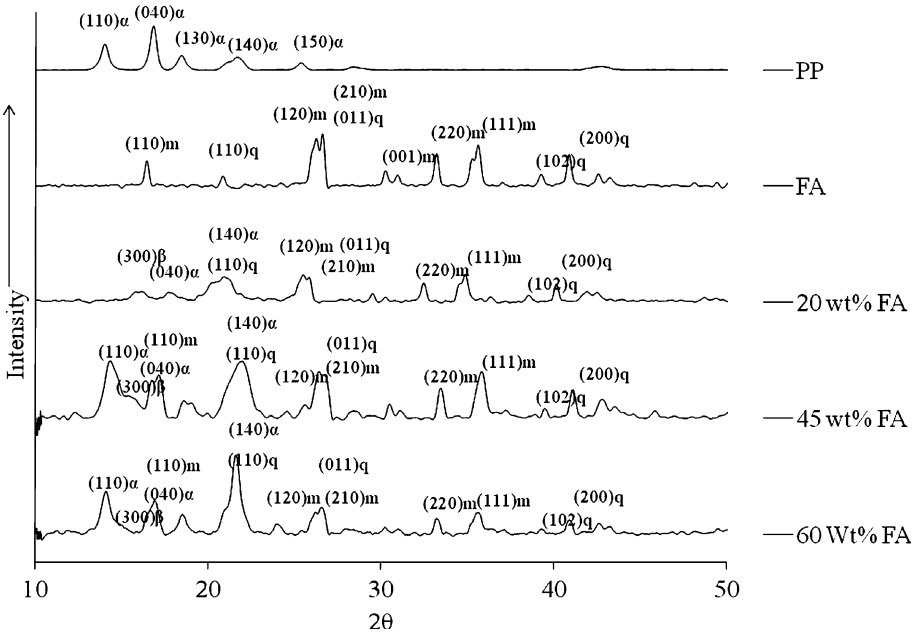

Fig. 3 XRD spectra of neat PP, FA and composites of 20, 45 and 60% FA

Table 2 Thermal behaviour of polypropylene and polypropylene fly ash composite with different heating rates

FA (%)	Heating rate	Melting point α-phase	ΔH_m (J/g) α-phase	α-Phase (% X_α)	Melting point β-phase	ΔH_m (J/g) β-phase	β-Phase (% X_β)
0	10	165.0	77.84	44	136.6	0.51	0.3
	15	164.6	70.25	39	136.6	0.25	0.2
	20	163.1	45.21	25	136.4	0.13	0.2
20	10	166.4	61.52	35	132.4	1.66	1.0
	15	163.6	58.73	32	131.6	0.52	0.8
	20	163.4	42.59	24	130.4	1.07	0.7
45	10	163.4	41.75	24	132.7	17.13	11
	15	162.1	32.59	19	131.1	12.09	8
	20	162.1	31.56	17	131.1	12.19	7
60	10	168.4	28.15	16	135.4	4.56	3
	15	162.6	21.55	12	133.1	3.15	2
	20	162.7	20.36	11	132.1	3.44	2

(c) The melting point, enthalpy, crystallinity and the concentrations of α- and β-crystalline phases steadily go down as DSC heating rate goes up, indicating that high heating rate inhibits equilibrium development in that. It does not allow enough time for the molecular movements of the polymer chains to happen.

Mechanical properties of PP–FA composites

The stress–strain diagrams of PP and composites at 25, 50 and 70 °C are presented in Figs. 5, 6, and 7. The calculated values of tensile strength, strain to failure, and percentage change in modulus of the materials are given in Table 3. The modulus values presented in Table 3 as obtained the data file- in the absence of an extensometer- appears to be somewhat lower than published values, perhaps showing a systematic error. (The modulus values of neat PP shown in Table 3 match with published literature who have used a

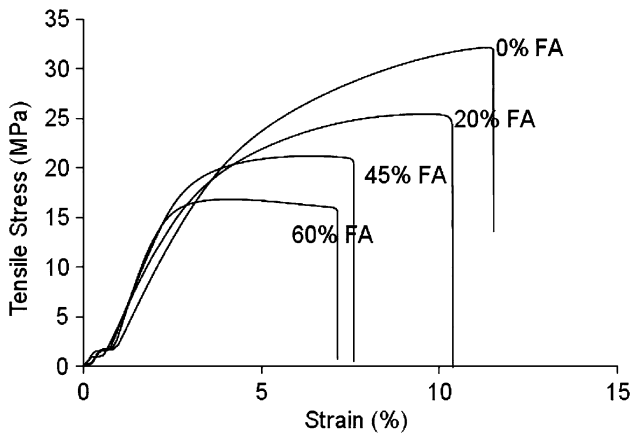

Fig. 5 Stress–strain relationship of PP and composites at test temperature 25 °C

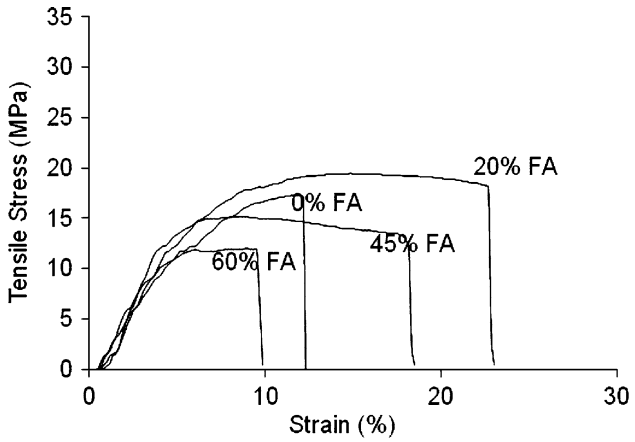

Fig. 6 Stress–strain relationship of PP and composites at test temperature 50 °C

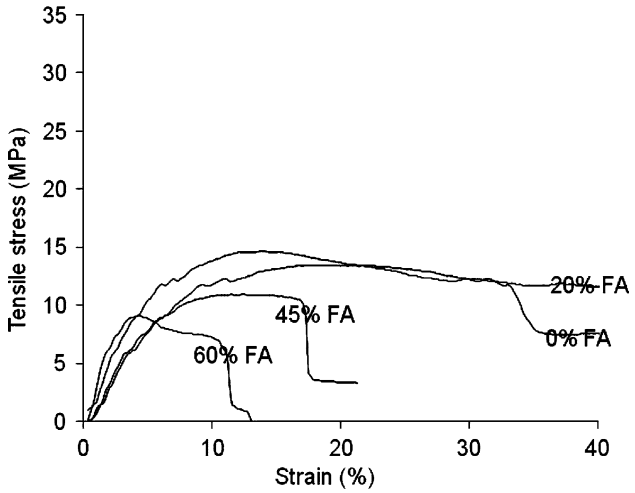

Fig. 7 Stress–strain relationship of PP and composites at test temperature 70 °C

Table 3 Mechanical properties of polypropylene–fly ash composites

FA (%)	Test temp. (°C)	Tensile stress (MPa)	Strain at failure (%)	Modulus (MPa)	Increase in modulus (%)	Interfacial parameter (B_y)
0	25	32.2 ± 0.8	11.5 ± 0.2	528	–	–
20	25	25.4 ± 0.5	11.0 ± 0.4	578	9 ± 0.6	1.5
45	25	21.2 ± 0.7	7.6 ± 0.2	650	23 ± 0.5	1.7
60	25	17.0 ± 0.6	6.5 ± 0.3	657	25 ± 0.4	1.7
0	50	17.3 ± 0.5	12.2 ± 0.5	238	–	–
20	50	19.5 ± 0.5	22.5 ± 0.5	268	12 ± 0.7	4.1
45	50	15.0 ± 0.5	18.0 ± 0.5	278	24 ± 0.4	2.6
60	50	12.0 ± 0.5	9.6 ± 0.5	306	29 ± 0.5	2.3
0	70	13.0 ± 0.5	44.0 ± 0.5	170	–	–
20	70	14.7 ± 0.5	51.5 ± 0.5	185	9 ± 0.6	4.1
45	70	11.0 ± 0.5	23.5 ± 0.5	261	53 ± 0.6	2.5
60	70	9.1 ± 0.5	12.8 ± 0.5	270	59 ± 0.7	2.3

Volume fraction (ϕ_f) was calculated with equation in Ref. [32] and the values were found for the composite 20% FA, 0.14, 45% FA composite, 0.34 and 60% FA composite, 0.49. Modulus values were calculated from the linear regions of stress–strain curves without any extensometer

similar computerised system [32]). As our main interest is in the percentage change of modulus as a function of temperature and fly ash content, these, as included in Table 3, agree with the literature [11].

Generally the tensile strength of the composites are lower than neat resins, the drop increasing with increase of FA content, as reported in the literature [11] and Fig. 5 shows the same behaviour at 25 °C test temperature. The lowering nature of tensile strength with 20% FA increased further in Figs. 6 and 7 at test temperatures 50 and 70 °C.

In Fig. 8 and between 0 and 60% loadings of FA, the drop in failure strength is linear at 25 °C, which implies that, in the absence of a chemical bonding between FA and PP. In higher FA additions, lager defects are created, which increase in the material linear elastic fracture mechanics type of failure [18]. At 50 and 70 °C, similar linear drop in strength is observed between 20 and 60% FA. However, between 0 and 20% FA, there is a small yet noticeable increase in the strength, which could be attributed to the enhanced free volume of the thermoplastic polymer at the elevated temperature, which is being filled up by the fly ash apparently causing preferable wetting between the PP and the FA, thereby increasing the strength. The system of talc and PP composite showed the similar behaviour. The embedment of talc in void sites in PP enhanced the adhesion exceptionally with PP and gave the high performance of mechanical strength [33]. In the reduction of free volume environment, the segmental chain of PP gets restriction strongly, reflecting higher T_g values. The details of dynamic mechanical behaviour in correlation with static will be reported shortly elsewhere.

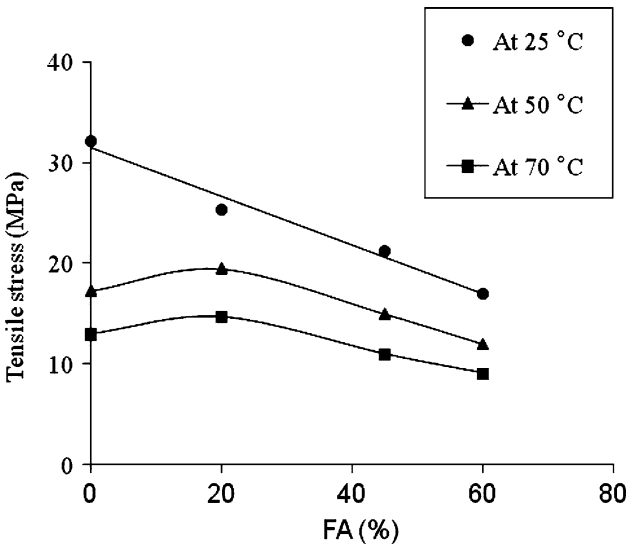

Fig. 8 Effect of FA concentration on tensile strength of composites at different test temperatures

The secondary binding forces –OH groups on the surface of FA may have a role in the formation of a weak interfacial interactions in PP chain [34, 35], which is supported by further by the calculation of interfacial parameter by conventional equation later. However, 20% FA seems to be the limiting amount that can be absorbed in the free volume expansion, and any further increase in FA content results in increased linear elastic fracture. The fact that all the three receding straight lines have very similar gradient confirms this proposition. Exceeding a 20% addition rate of may reduce intimate contact between the surface of FA and PP lessening the interfacial interaction [36].

The ductility of the materials ensured by strain failure at various temperatures is shown in Fig. 9. At 25 °C, ductility decreases linearly with FA addition, whereas at 50 and

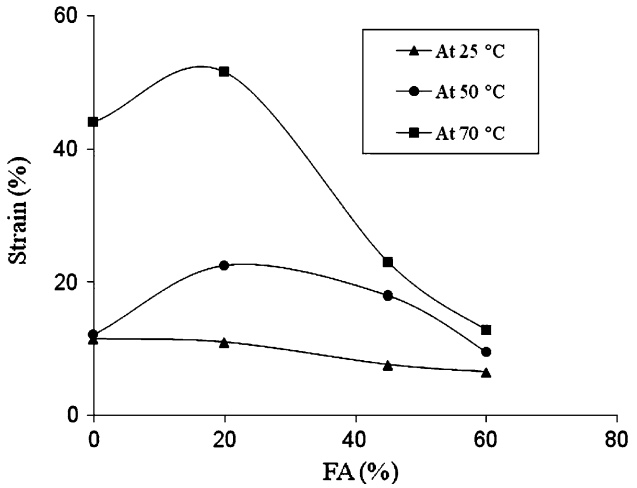

Fig. 9 Effect of FA concentration on the strain to failure of composites at different test temperatures

70 °C with the effect of the increase in the flow of PP the ductility shows a distinct improvement for 20% FA. Beyond the values of 20%, the ductility decreases—more or less linearly—with more FA addition. The mechanisms considered earlier for Fig. 8 could provide an explanation for these data.

Figure 10 represents an as-expected improvement in modulus of elasticity of the composites as a function of FA%, following the rules of mixture [37]. Further, as anticipated, increase in test temperature reduces the modulus [19]. The mechanical properties of PP as a function of its three crystalline forms monoclinic shape α-phase, hexagonal shape β-phase and triclinic shape γ-phase are reported in the literature [38].

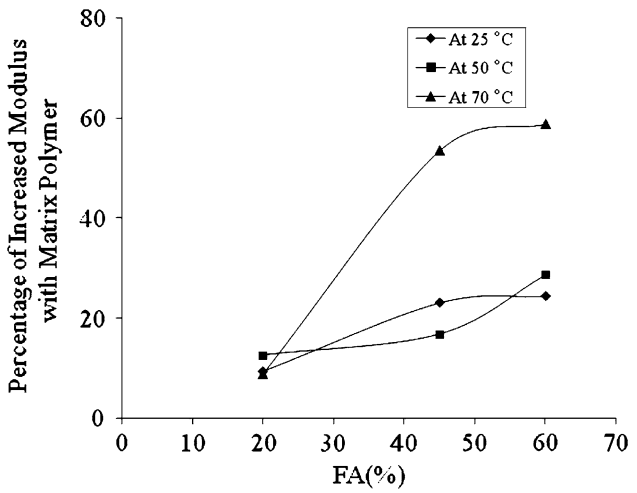

Fig. 10 Effect of FA concentration on percentage increase in modulus of composites at different test temperatures

SEM study of morphology from fracture surfaces

The SEM micrographs of fracture surfaces of PP and composites tested at 25, 50 and 70 °C are shown in Figs. 11, 12 and 13, respectively. From these figures, the following observations can be summarized:

(a) Figure 11a at 25 °C shows the presence of α-spherulite fragments, voids, and bundles of drawn fibrils in neat PP [39]. In Fig. 11b with 20% FA, it appears that a portion of the fly ash particles are occupying heterogeneous nucleus sites consequently giving PP–FA bonding interaction, which led to a significant increase in strain to failure, as seen in Fig. 9. For 45 and 60% FA composite the excess FA are obviously occupying sites within the spherulites and in-tersph-erulitic boundaries. In the absence of any chemical bonding agent as in this case, FA particles were separated cleanly from the PP surface, as evident in Fig. 11c, d. The polymer fibrillation happens at a considerably lower applied stress, because the spherical FA particles can raise the localised stress by a factor as high as 3, thereby reducing the overall strength of the composites, as seen in Fig. 8.

(b) At 50 °C there is evidence of fragmentation, voids and more fibrillar flow of the polymer chains (Fig. 12a). In 20% FA composites (Fig. 12b), the PP fibrils appear to fully cover the FA particles that are within the spherulites. The phenomenon supports the presence of physical interaction between FA and PP chain. Increasing FA content to 45 and 60% (Fig. 12c, d) shows some evidence of the polymer fibril wetting the FA surface.

(c) Figure 13a–d at 70 °C support the enhancement of the phenomena as observed at 50 °C and shown in Fig. 12. The fact that at 20% FA particles are separated and entirely covered with PP versus higher percentage of FA where the ash particles are in closer proximity is also relevant. Once in close proximity the ash particles can act on each other mechanically as levers transferring additional strain to the more diluted PP matrix as the composite is placed under mechanical load.

Correlation of mechanical properties with interfacial interaction parameter

The formation and development of interfacial interactions between filler and polymer in composites are critical in engineering application of composite materials. Composites that are more rigid have superior interfacial interaction due to superior transfer load from matrix to filler. Although the measurement of interfacial adhesion is an important

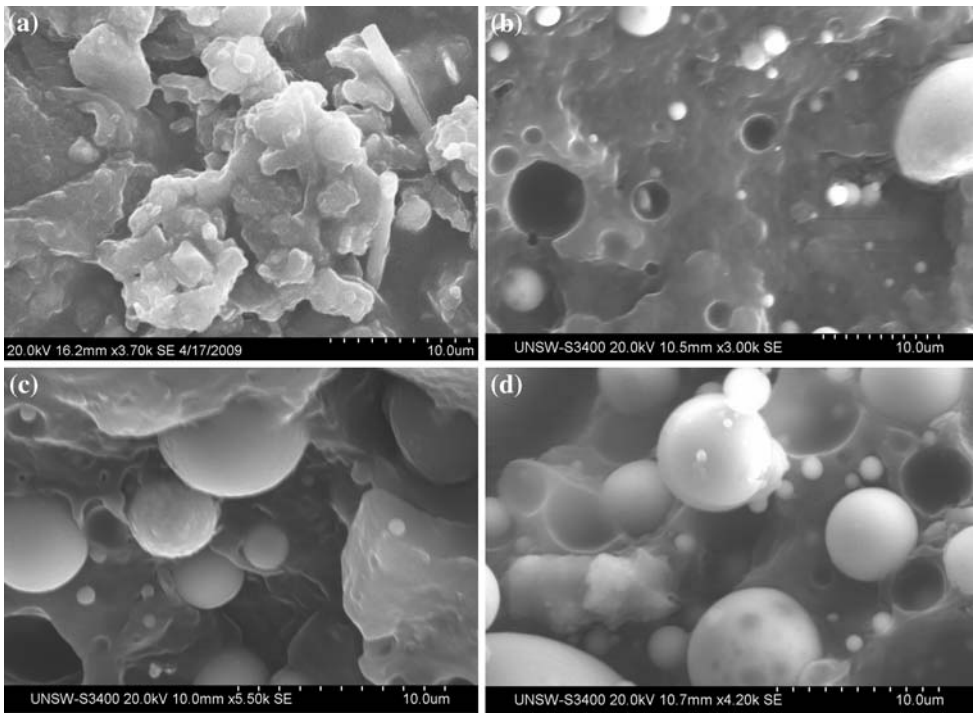

Fig. 11 SEM images of fractured surface of neat PP and composites at 25 °C, **a** neat PP showing compact pellet structure, **b** 20% showing homogeneous dispersion of FA, **c** 45% showing a saturated level FA and **d** 60% illustrating highly populated FA and minimum intimate contact area to PP

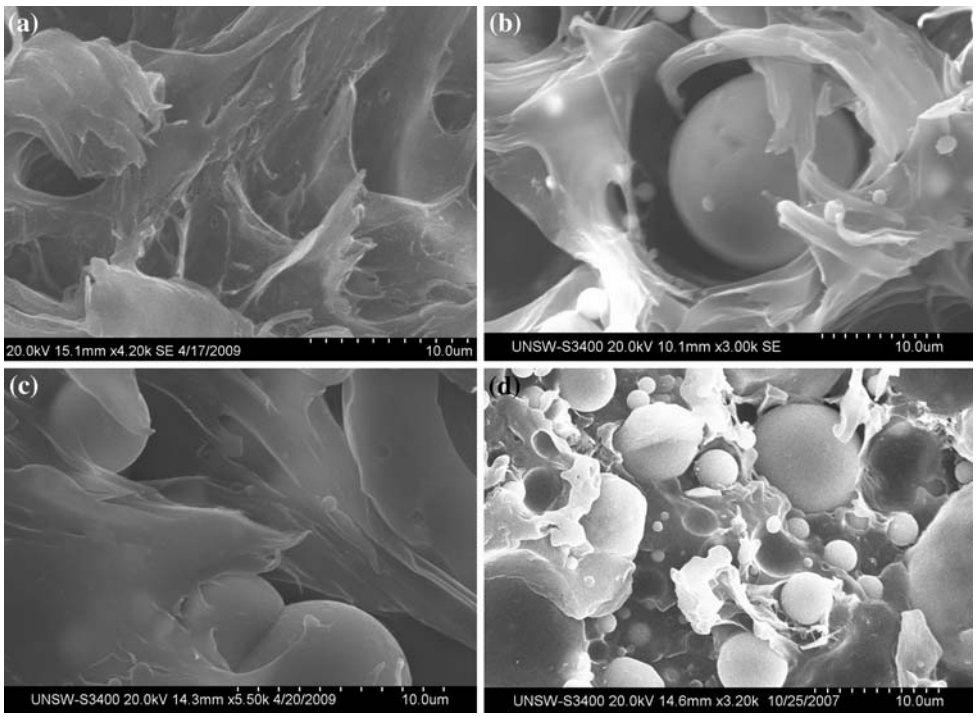

Fig. 12 SEM images of fractured surface of neat PP and composites at 50 °C, **a** neat PP showing extended flow of PP chain, **b** 20% showing fully covered FA by PP, **c** 45% existing interfacial linking between FA and PP resulting in crack prppagation along poles [43] and **d** 60% FA showing majority of debonded FA particles in fracture surface

task in the development of composites, the absolutely quantification of interfacial interaction is complicated. Pukanszky et al. have reported an empirical Eq. 2 [29, 33] in relation with tensile strength to calculate the interfacial interaction, B_y between the filler and matrix by numerical values.

$$\delta_c = \delta_0(1-\phi_f)/(1+2.5\phi_f)\exp(B_y\phi_f) \quad (2)$$

where δ_c and δ_0 are the yield stresses of the composite and polymer matrix, respectively, ϕ_f the volume fraction of the filler, calculated from the weight fraction. Higher values of B_y imply higher yield strength whilst lower values indicate

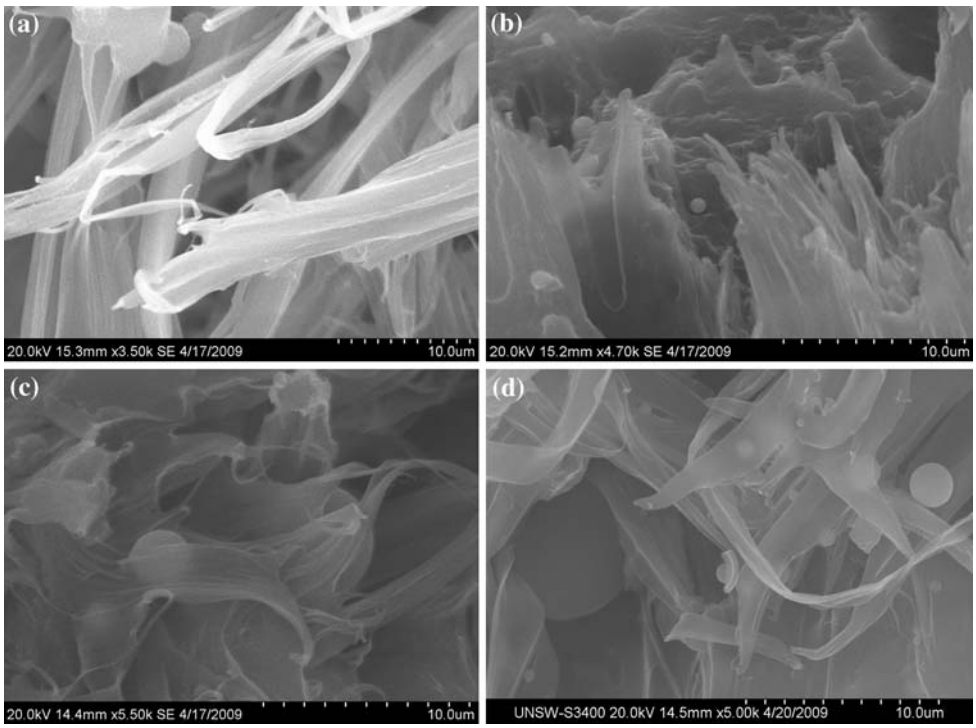

Fig. 13 SEM images of fractured surface of neat PP and composites at 70 °C, **a** neat PP showing deformed fibrils, **b** 20% ductile failure, most FA particles apparently being covered by polymer lamellae, **c** 45% evidence of bonding between FA and PP and ductile mode of crack propagation and **d** 60% FA showing plastic deformation, and some debonded FA particles

materials having comparatively weaker strength composites [33].

Using Eq. 2, Pukanszky parameter B_y, has been calculated, and presented in Table 3, which are similar to those reported by Rong et al. [29] and Leong et al. [39] in their composite systems using reinforcement such as calcium carbonate, talc and kaolin. This implies that Pukanszky parameter B_y is a universal concept in particle filled composites.

Figure 14 shows the plot of ductility as a function of the Pukanszky parameter. Considering that composites

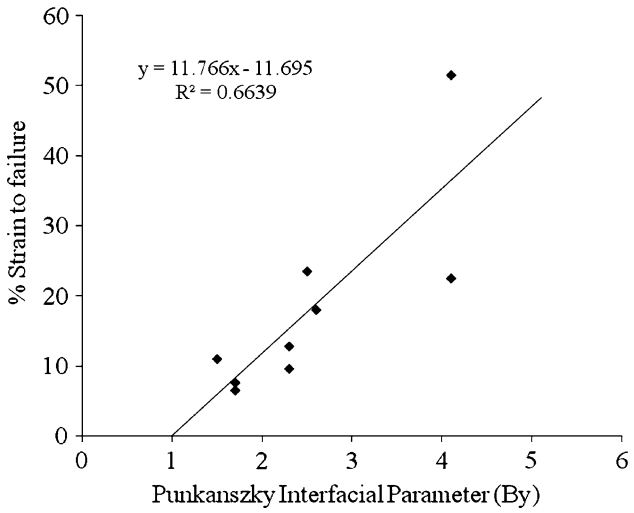

Fig. 14 Relationship between failure strain and Pukanskzy interfacial interaction parameter in composites

interface is a very complex quantity involving many parameters such as chemistry of the constituents, surface inductive forces, wettability, secondary bonding, as well as mechanical interlocking, as reported by recent quantitative atomic force microscopic studies on number of composite systems [40, 41], a straight line as illustrated in Fig. 14 is a good agreement. SEM pictures presented above support this argument.

Interpretation of formation of interfacial interaction

Under atmospheric condition, a common functional hydroxyl (–OH) group or ion in general covers the surfaces of metal and metalloid oxides, which has significant role in the formation of physical bonding to the surfaces of substrates. The presence of –OH in fully hydroxyl ted silica powder has been identified elsewhere [34, 35].

As the major ingredients of FA are oxides of silicon, aluminium-mullite and α-quartz, therefore, we have made an attempt to examine the presence level of –OH group on the FA surface by XPS method, as shown in Fig. 15 in the range of binding energy 95–110 eV. Clearly combined peaks of –OH and –O– attached to α-quartz SiO_2 and mullite are present at the binding energy 103.7 eV. The –OH group on the surface of FA is considered in the formation of interfacial interactions with PP chain, as also is evident in Figs. 12b, c and 13b, c. Future work will use a bonding agent to improve chemical adhesion between PP and FA. It is clear that there is a need to explore the behaviour of FA in composites at 15–20 25–30% perhaps

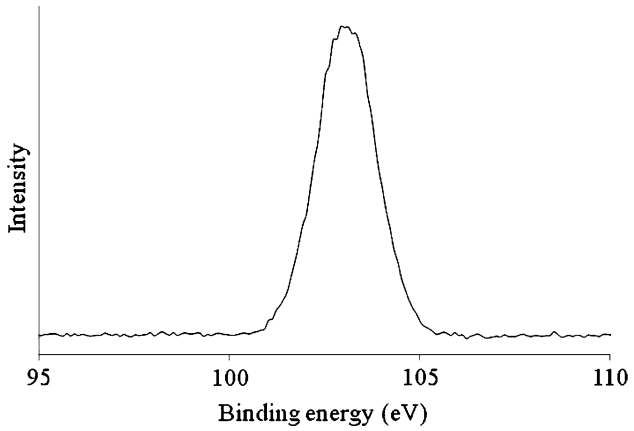

Fig. 15 XPS spectra of FA showing a combined peak of hydroxides and oxides of silicon

to see clearly, where the beneficial interaction starts and finishes. 20–45% is quite a big jump, appropriate in this study but the trend shapes and directions in the lower % need to be demonstrated.

Impact test

The average energy of neat PP and composites were presented in Fig. 16 at test temperatures 25, 50 and 70 °C as a function of fly ash content.

Generally speaking, the impact energy—which matches with literature [42], (a) increased with increasing test temperature and (b) depended on the percentage of FA. The maximum gain was 58% for the composite with 45% FA, tested at 70 °C, compared to that of pure PP tested at 25 °C.

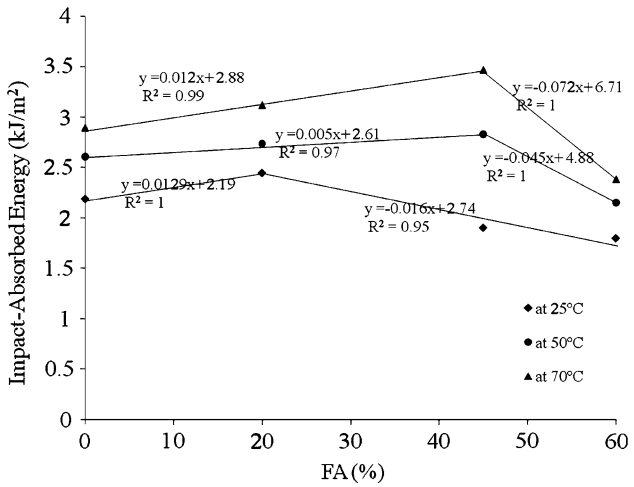

Fig. 16 Impact absorbed energy of PP and composite samples at three different temperatures as function of % FA—the equations representing the linear increase and decrease of the impact energy as a function of FA content

According to literature [43], the enhancement of impact fracture energy is due to the improvement of adhesion at the interface of the polymer and the filler particles. The increased impact energy at 50 and 70 °C is consistent with the tensile study results, Figs. 5, 6 and 7, which is considered due to increased bonding between the filler and matrix. As the test, temperature increases the fracture phenomena will change from brittle to ductile due to increased mobility of the polymer chains causing rearrangement of the adhesion of fly ash. In this improved ductile mode, energy is also absorbed in the process of plastic deformation of matrix at spherical fly ash/PP interface. Tan and Mchugh [44] observed the existence of interstitial voids between spherical filler and matrix particles, which under impact loading act as initiators of crack initiation and growth. In the present study, SEM images of fractured surface of impact test shown for the matrix and three composites at 70 °C in Fig. 17 which supports a combination of the two processes, i.e. the plasticity of the polymer at elevated temperature, and crack initiation and growth due to the spherical fillers. The presence of partially bonded and partially clean separated particles (Fig. 17b–d) indicates that FA particles have a mixed range of attachment to PP chains [43]. With 60% FA, the fraction of unbonded particles is logically higher thereby resulting a decrease in impact strength. Because the notch tip of the impact sample has a defined roundness according to the standard, significant amount of energy is consumed in the initiation stage [45]. At elevated temperature, the polymer chains are more plastic (Fig. 9). If one ignores the effect of high strain rate under impact, the plasticization would still result in higher initiation region.

Conclusions

The following conclusions are reached from this work:

(a) The melting point, enthalpy, crystallinity and the concentrations of α- and β-crystalline phase steadily go down with heating rate going up.
(b) A maximum 11% β form crystallinity has been achieved by 45% FA.
(c) At 25 °C tensile strength decreases with fly ash content, whereas at 50 and 70 °C there is initial increase in strength up to 20% FA, but after that strength goes down with more FA addition: linear drop in strength is observed between 20 and 60% FA. The drop in strength with addition of fly ash is believed to be due to stress concentration effect or formation of weak interface.
(d) Fracture surfaces of neat PP show α-spherulite fragments, voids, and bundles of drawn fibrils. With

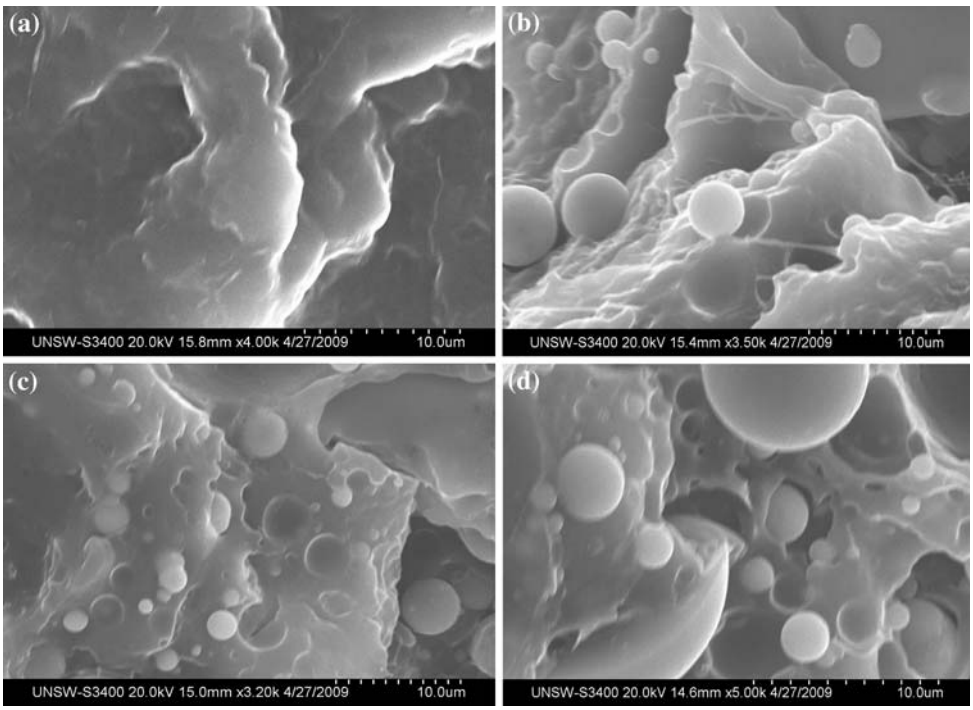

Fig. 17 SEM images of impact fracture surface of neat PP and composites at 70 °C, **a** neat PP showing plasticised lamellar deformation, **b** 20%, **c** 45% and **d** 60% FA composites partially bonded and debonded features in three composite samples

FA addition, a portion of the fly ash particles acts as heterogeneous nucleation sites giving PP-FA interactive physical bonding, the remainder of the FA occupying sites within the spherulites and intersperulitic boundaries.

(e) At 50 and 70 °C, more fibrillar flow of polymer chains is evident.

(f) Existence of OH group on the surface of FA is considered a plausible way for formation of interfacial interaction with PP chain.

(g) At 25 °C, Pukanszky interfacial interaction parameter B_y was calculated to be in the range of 1.5–1.7 for all composites with FA. At 50 and 70 °C the value went up to 4.1 with 20% FA and it was this composite, which gave the highest strain to failure.

(h) The higher impact-absorbed energies at elevated temperatures may have resulted from a combination of plastic flow and good adhesion between fly ash and PP.

Acknowledgements The authors are grateful to the help and cooperation of Dr. Norman Booth, Department of Chemistry, Materials and Forensic Science, University of Technology, Sydney, NSW 2000, Australia in providing Instron for tensile strength at elevated temperature. The authors are also grateful to Australian Research Council for the financial support of this work.

References

1. Iyer RS, Scott JA (2001) Resour Conserv Recyl 31:217
2. Gomes S, Francois M, Abdelmoula M, Refait P, Pellissier C, Evrard O (1999) Cem Concr Res 29:1705
3. Demanet CM (1995) Appl Surf Sci 89:97
4. Kutchko BG, Kim AG (2006) Fuel 85:2537
5. Ward CR, French D (2006) Fuel 85:2268
6. McDowell RW (2005) Aust J Soil Res 43:853
7. Gorninski JP, Molin DCD, Kazmierczak CS (2004) Cem Concr Res 34:2091
8. Kojima Y, Usuki A, Kawasumi M, Fukushima Y, Okada A, Kurauchi T, Kamigaito O (1993) J Mater Res 8:1179
9. Guhanathan S, Sarojadevi M (2004) Compos Interface 11(1):43
10. Gupta N, Brar BS, Woldesenbet E (2001) Bull Mater Sci 24(2):219
11. Wong KWY, Truss RW (1994) Comp Sci Technol 52:361
12. Wang M, Shen Z, Cai C, Ma S, Xing Y (2004) J Appl Polym Sci 92:126
13. Jarvela PA, Jarvela PK (1996) J Mater Sci 31:3853. doi: 10.1007/BF00352802
14. Huang X, Hwang JY, Gillis JM (2003) J Miner Mater Charact Eng 2(1):11
15. Okamoto M, Nam PH, Maiti P, Kotaka T, Hasegawa N, Usuki A (2001) Nano Lett 1(6):295
16. Tjong SC, Li RKY, Cheung T (1997) Polym Eng Sci 37(1):166
17. Bigg DM (1987) Polym Compos 8(2):115
18. Li JX, Silverstein M, Hiltner A, Baer E (1994) J Appl Polym Sci 52:255
19. Brydson JA (2001) Plastics materials. Butterworth-Heinemann, Oxford, Boston, Elsiver Science. ISBN: 0750618647
20. Lotz B, Wittmann JC, Lovinger JA (1996) Polymer 37(22):4979
21. Liu J, Wei X, Guo Q (1990) J Appl Polym Sci 41:2829
22. Ferrage E, Martin F, Boudet A, Petit S, Fourty G, Jouffet F, Micoud P, Parseval PD, Salvi S, Courgerette C, Ferret J, Saint-Gerard Y, Buratto S, Fortune JP (2002) J Mater Sci 37:1561. doi: 10.1023/A:1014929121367
23. Mucha M, Krolikowski Z (2003) J Therm Anal Calorim 74:549
24. Chen J, Li X, Wu C (2007) Polym J 39(7):722
25. Zhang QX, Yu ZZ, Xie XL, Mai YW (2004) Polymer 45:5985
26. Kim B, Lee SH, Lee D, Ha B, Park J, Char K (2004) Ind Eng Chem Res 43:6082
27. Tang J, Wang Y, Liu HY, Belfiore LA (2004) Polymer 45:2081
28. Gaceva GB, Janevsky A, Mader E (2001) Polymer 42:4409

29. Rong MZ, Zhang MQ, Pan SL, Lehmann B, Friedrich K (2004) Polym Int 53:176
30. Valentini L, Biagiotti J, Kenny JM, Santucci S (2003) J Appl Polym Sci 87:708
31. Xie XL, Li RKY, Jong SC, Mai YW (2002) Polym Compos 23(3):319
32. Yuan Q, Misra RDK (2006) Polymer 47:4421
33. Leong YW, Bakar MBA, Ishak ZAM, Ariffin A, Pukanszky B (2004) J Appl Polym Sci 91:3315
34. Mueller R, Kammler HK, Wegner K, Pratsinis SE (2003) Langmuir 19:160
35. Paparazzo E (1996) Surf Interface Anal 24:729
36. Nielsen LE (1966) J Appl Polym Sci 10:97
37. Tsai SW (1988) Composite design. Think Composites Press, Dayton, OH
38. Kinloch AJ (1987) Rubber-toughened plastics. American Chemical Society, Washington, DC, pp 67–91. ISBN: 0841214883
39. Bandyopadhyay S, Brown HR (1981) Polymer 22:245
40. Anandhan S, De PP, Bhowmick AK, De SK (2003) J Appl Polym Sci 90:2348
41. Ghosh A, Rajeev RS, Dey SK, Sharp W, Bandyopadhyay S (2006) J Elastomers Plast 38:119
42. Weon JI, Sue HJ (2006) J Mater Sci 41:2219. doi:10.1007/s10853-006-7171-x
43. Spanoudakis J, Young RJ (1984) J Mater Sci 19:487. doi:10.1007/BF00553571
44. Tan LS, Mchugh AJ (1996) J Mater Sci 31:3701. doi:10.1007/BF00352783
45. Bandyopadhyay S (1990) Mater Sci Eng A 125:157